J. Phys.: Condens. Matter **21** (2009) 056004 (8pp) doi:10.1088/0953-8984/21/5/056004

# Understanding the inverse magnetocaloric effect in antiferro- and ferrimagnetic arrangements

**P J von Ranke[1,4], N A de Oliveira[1], B P Alho[1], E J R Plaza[1,2], V S R de Sousa[1], L Caron[2] and M S Reis[3]**

[1] Instituto de Física 'Armando Dias Tavares', Universidade do Estado do Rio de Janeiro—UERJ, Rua São Francisco Xavier, 524, 20550-013, RJ, Brazil
[2] Instituto de Física 'Gleb Wataghin', Universidade Estadual de Campinas—UNICAMP, 13083-970 Campinas, SP, Brazil
[3] CICECO, Universidade de Aveiro, 3810-193 Aveiro, Portugal

E-mail: von.ranke@uol.com.br

Received 28 September 2008, in final form 12 December 2008
Published 12 January 2009
Online at stacks.iop.org/JPhysCM/21/056004

**Abstract**
The inverse magnetocaloric effect occurs when a magnetic material cools down under applied magnetic field in an adiabatic process. Although the existence of the inverse magnetocaloric effect was recently reported experimentally, a theoretical microscopic description is almost nonexistent. In this paper we theoretically describe the inverse magnetocaloric effect in antiferro- and ferrimagnetic systems. The inverse magnetocaloric effects were systematically investigated as a function of the model parameters. The influence of the Néel and the compensation temperature on the magnetocaloric effect is also analyzed using a microscopic model.

## 1. Introduction

Intensive investigations have been concentrated on the magnetocaloric effect (MCE) since 1997, when Pecharsky and Gschneidner reported [1] the discovery of the giant magnetocaloric effect in $Gd_5(Si_xGe_{1-x})_4$. This discovery was a significant breakthrough since before the giant-MCE discovery, the main interest in the MCE was restricted to producing refrigeration in very low temperatures [2, 3]. Several giant magnetocaloric materials have been reported since then, such as $MnFeP_{0.45}As_{0.55}$ [4], $MnAs_{1-x}Sb_x$ [5, 6], and $La(Fe_{1-x}Si_x)_{13}$ [7, 8]. Theoretical models in which the magnetoelastic interaction is considered, in the Bean and Rodbell [9] assumption, were successfully [10–12] applied to the giant-MCE in $Gd_5(Si_xGe_{1-x})_4$, $MnFeP_{0.45}As_{0.55}$ and $MnAs_{1-x}Sb_x$. Recently review articles on magnetocaloric materials have been elaborated by: Brük [13], Pecharsky *et al* [14], and Phan and Yu [15].

The MCE is characterized by the isothermal magnetic entropy change $\Delta S$ and the adiabatic temperature change $\Delta T_{ad}$, which are observed upon magnetic field changes. If the temperature derivative of the magnetization is negative, as is the case of the regular ferromagnetic materials, the thermodynamic formulation of the $\Delta S$ and $\Delta T_{ad}$ predicts $\Delta S < 0$ and $\Delta T_{ad} > 0$ (the direct MCE), i.e. the sample heats up when the external magnetic field is applied adiabatically. On the other hand, if the temperature derivative of the magnetization is positive, an opposite effect occurs, i.e. $\Delta S > 0$ and $\Delta T_{ad} < 0$ (the inverse MCE), the sample cools down when the external magnetic field is applied adiabatically. The inverse MCE exists in different kinds of magnetic arrangements. In the *antiferromagnetic* compound $MnBr_2{\cdot}4H_2O$ an inverse MCE of about $\Delta T_{ad} \approx -0.125$ K at $T = 1.75$ K was observed [16, 17], under magnetic field change of 1 T. The inverse MCE in antiferromagnetic compounds is associated with antiparallel disorder of magnetic sublattices and was first noted by Kurti [18] and Garrett [19] in connection with the studies of a Tutton salts. In the *ferrimagnetic* compound ytterbium iron garnet $Yb_3Fe_5O_{12}$ the magnetocaloric measurements [20] showed that as the

[4] Address for correspondence: Instituto de Física—Departamento de Eletrônica Quântica, Universidade do Estado do Rio de Janeiro, Rua São Francisco Xavier, 524-3$^0$ andar. Maracanã-Rio de Janeiro–20550-013, Brazil.

 

magnetic field is increased from zero to 6.5 T the temperature of the compound falls from 22 to 16.5 K, i.e. an inverse MCE of $\Delta T_{ad} = -5.5$ K. In the *paramagnetic* compound $PrNi_5$ heat capacity measurements showed [21, 22] the inverse MCE with maximum value of about $\Delta T_{ad} \approx -0.7$ K which occurs at 6.5 K, under magnetic field change from zero to 5 T. Recently, giant inverse MCE was reported [23, 24] in *ferromagnetic* Heusler-type alloys $Ni_{0.5}Mn_{0.5-x}Sn_x$. For $x = 0.13$ the maximum entropy change of $\Delta S = 18$ J kg$^{-1}$ K$^{-1}$ was obtained at about $T = 300$ K for magnetic field change from zero to 5 T. The intensity of this inverse MCE is almost equal to the direct giant-MCE measured in $Gd_5Si_2Ge_2$ [25]. There are several other materials in which inverse MCEs were recently observed, some examples are: $Ni_{50}Mn_{34}In_{16}$ [26]; CoMnSi [27]; and $Mn_{1.82}V_{0.18}Sb$ [28].

In this paper a microscopic model has been developed to quantitatively understand the inverse MCE which can appear in antiferromagnetic and ferrimagnetic arrangements. The model takes into account a magnetic system formed by two different magnetic ions which are coupled by the exchange interactions. A general magnetic state equation was obtained from the microscopic Hamiltonian. The influence of the exchange interactions on the magnetocaloric potential was investigated, highlighting the inverse MCE due to the antiferromagnetism and ferrimagnetism with and without compensation temperature.

## 2. Theory

In our model the magnetic system is formed by two sublattices of spins $J^a$ and $J^b$ in the presence of external magnetic field and in thermodynamic equilibrium. The Hamiltonian for this system is given by:

$$H = -\sum_{i,j} \lambda_{ab}^{(i,j)} J_i^a J_i^b - \sum_{i,j} \lambda_{aa}^{(i,j)} J_i^a J_i^a - \sum_{i,j} \lambda_{bb}^{(i,j)} J_i^b J_i^b - \mu_B h \sum_i (g_a J_i^a + g_b J_i^b), \quad (1)$$

where $\lambda_{ab}^{(i,j)}$, $\lambda_{aa}^{(i,j)}$, and $\lambda_{bb}^{(i,j)}$ are the inter- and intra-sublattices exchange parameters between pairs of magnetic ions. $J^a$, $J^b$, $g_a$, and $g_b$ represent the total angular momentum operators and the Landé factors of the $a$-ions and $b$-ions. The last term accounts for the Zeeman interaction, where $h$ is the external magnetic field and $\mu_B$ is the Bohr magneton. Extracting from (1) the single ion Hamiltonian for the nearest and next nearest neighbor pairs, we have:

$$H = -\lambda_{ab} J_i^a \sum_{j=1}^{Z_{ab}} J_j^b - \lambda_{ab} J_i^b \sum_{j=1}^{Z_{ba}} J_j^a - \lambda_{aa} J_i^a \sum_{j=1}^{Z_{aa}} J_j^a - \lambda_{bb} J_i^b \sum_{j=1}^{Z_{bb}} J_j^b - \mu_B h (g_a J_i^a + g_b J_i^b), \quad (2)$$

where the sums are over the $Z_{ab}$ nearest $J_j^b$-neighbors of the $J_i^a$ ion, $Z_{ba}$ nearest $J_j^a$-neighbors of the $J_i^b$ ion, $Z_{aa}$ nearest $J_j^a$-neighbors of the $J_i^a$ ion and $Z_{bb}$ nearest $J_j^b$-neighbors of the $J_i^b$ ion, respectively. $\lambda_{ab}$, $\lambda_{aa}$, and $\lambda_{bb}$ are the exchange interactions between nearest inter-sublattices neighbors, the exchange interactions between nearest intra-$a$-sublattice and $b$-sublattice neighbors, respectively. Considering that all ions in the $a$-sublattice, as well as the ions in the $b$-sublattice, are identical and equivalents, in the mean field approximation, we obtain:

$$H = -\lambda_{ab} Z_{ab} \langle J^b \rangle J^a - \lambda_{ab} Z_{ba} \langle J^a \rangle J^b - \lambda_{aa} Z_{aa} \langle J^a \rangle J^a - \lambda_{bb} Z_{bb} \langle J^b \rangle J^b - \mu_B h (g_a J^a + g_b J^b). \quad (3)$$

The $\langle J^a \rangle$ and $\langle J^b \rangle$ quantities are directly related with the magnetization on the $a$, $b$-sublattices:

$$M_\delta = N_\delta g_\delta \mu_B \langle J^\delta \rangle. \quad (4)$$

Here $\delta = a, b$ is the sublattice index. In our magnetic lattice there are $N_a = pN$ magnetic atoms of kind $J^a$ and $N_b = qN$ atoms of kind $J^b$ (here $N$ is the total number of magnetic atoms, $p$ is the fraction of magnetic atoms on $a$-sites and $q = 1 - p$ is the fraction of magnetic atoms on $b$-sites). The Hamiltonian (3) can be written as:

$$H = -\mu_B g_a h_a J^a - \mu_B g_b h_b J^b, \quad (5)$$

with

$$h_a = h + \gamma_{ab} M_b + \gamma_{aa} M_a, \quad (6)$$

$$h_b = h + \gamma_{ba} M_a + \gamma_{bb} M_b, \quad (7)$$

where $\gamma_{ab} = \lambda_{ab} Z_{ab}/(N_b g_a g_b \mu_B^2)$, $\gamma_{ba} = \lambda_{ab} Z_{ba}/(N_a g_a g_b \mu_B^2)$, $\gamma_{aa} = \lambda_{aa} Z_{aa}/(N_a g_a^2 \mu_B^2)$ and $\gamma_{bb} = \lambda_{bb} Z_{bb}/(N_b g_b^2 \mu_B^2)$ are the proper normalized exchange parameters. It can be shown [29] from the general arguments that $\gamma_{ab} = \gamma_{ba}$.

Using the energy eigenvalues and eigenvectors of the Hamiltonian (5) the mean value quantities $\langle J^a \rangle$ and $\langle J^b \rangle$ from relation (4) can be calculated, leading to the following coupled magnetic state equations

$$M_a = pN\mu_B g_a J_a B_J \left[\mu_B g_a J_a h_a / kT\right], \quad (8)$$

$$M_b = qN\mu_B g_b J_b B_J \left[\mu_B g_b J_b h_b / kT\right]. \quad (9)$$

Where $B_J$ is the Brillouin function, $J_a$ and $J_b$ are the total angular momentum numbers, and $k$ is the Boltzmann constant.

The magnetization curves $M = M_a + M_b$ that emerge as the solution from the magnetic state equations (8) and (9) can present several different profiles. Depending on the chosen set of exchange parameters $[\gamma_{ab}, \gamma_{aa}, \gamma_{bb}]$, the ionic parameters $[g_a, J_a, g_b, J_b]$ and the fraction of magnetic ions of $a$-kind and $b$-kind $[p, q]$ the magnetic structure configurations ferrimagnetic (FI), antiferromagnetic (AF), and ferromagnetic (FE) can be obtained. The transition temperature from these ordered phases to paramagnetic (PA) phase can be obtained analytically from the magnetic state equations and is given by

$$T_{FI} = \frac{1}{2}\left[(pC_a\gamma_{aa} + qC_b\gamma_{bb}) + \sqrt{(pC_a\gamma_{aa} - qC_b\gamma_{bb})^2 + 4pqC_aC_b\gamma_{ab}^2}\right], \quad (10)$$

where $C_a = g_a^2\mu_B^2 J_a(J_a+1)/3k$ and $C_b = g_b^2\mu_b^2 J_b(J_b+1)/3k$ are the Curie constants. A particular case of relation (10)

is obtained considering $p = q = 1/2$, $C_a = C_b = C$, and $\gamma_{aa} = \gamma_{bb}$ which leads to the well know Néel temperature

$$T_{\mathrm{AF}} = \frac{C(\gamma_{aa} + |\gamma_{ab}|)}{2}, \tag{11}$$

and the simplest case occurs considering $\gamma_{aa} = \gamma_{ab} = \gamma$, in relation (11), which leads to the (FE)–(PA) phase transition at the Curie temperature $T_{\mathrm{FE}} = C\gamma$.

The magnetic entropy change $\Delta S$ versus $T$ in an isothermal process that occurs for magnetic field change ($h$: $0 \rightarrow h_0$) can be calculated by the integration of the Maxwell relation:

$$\Delta S = \int_0^{h_0} \left(\frac{\partial M}{\partial T}\right)_h \mathrm{d}h. \tag{12}$$

Under an adiabatic–isobaric process, the temperature change due to the change of the magnetic field ($h$: $0 \rightarrow h_0$) is obtained from the relation

$$\Delta T_{\mathrm{ad}} = -\int_0^{h_0} \frac{T}{C_h}\left(\frac{\partial M}{\partial T}\right)_h \mathrm{d}h, \tag{13}$$

where $C_h = C_h(h, T)$ is the total heat capacity at constant magnetic field and pressure. Usually in magnetic systems the two main contributions to $C_h$ are due to the crystal lattice $C_{\mathrm{l}} = C_{\mathrm{l}}(T)$ and the magnetic lattice $C_{\mathrm{m}} = C_{\mathrm{m}}(T, h)$. The first contribution is usually considered in the Debye approximation and the second one depends on the magnetic interactions taken into account in the model magnetic Hamiltonian.

Alternatively, from a theoretical point of view, the magnetic entropy can be directly calculated from the temperature derivative of the free energy. Using the Hamiltonian, the free energy is obtained:

$$F = -kTN_a \ln(Z_a) - kTN_b \ln(Z_b), \tag{14}$$

where $Z_a$ and $Z_b$ are the partition functions of the sublattices $a$ and $b$, respectively, and are given by:

$$Z_\delta = \frac{\sinh\left[\left(\frac{2J_\delta+1}{2J_\delta}\right)x_\delta\right]}{\sinh\left[\left(\frac{1}{2J_\delta}\right)x_\delta\right]}, \tag{15}$$

where $x_\delta = \mu_{\mathrm{B}} g_\delta J_\delta h_\delta / kT$. From the free energy (14), the magnetic entropy is obtained:

$$S(T, h) = R\left[p(\ln Z_a - x_a B_J(x_a)) + q(\ln Z_b - x_b B_J(x_b))\right], \tag{16}$$

where $R$ is the gas constant. In this way, relation (12) can also be expressed as:

$$\Delta S = S(T, h = h_0) - S(T, h = 0). \tag{17}$$

It is worth noticing that for high temperature, the Brillouin functions go to zero and the partition functions go to the total number of quantum magnetic states, i.e. $(2J_a + 1)$ and $(2J_b + 1)$ in the magnetic ions on sites $a$ and $b$, respectively in relation (16). Therefore, the maximum value of the magnetic entropy of the system formed by two sublattices with quantum total angular momentum $J_a$ and $J_b$ is given by:

$$S^{\mathrm{Max.}} = R\left[p\ln(2J_a + 1) + q\ln(2J_b + 1)\right]. \tag{18}$$

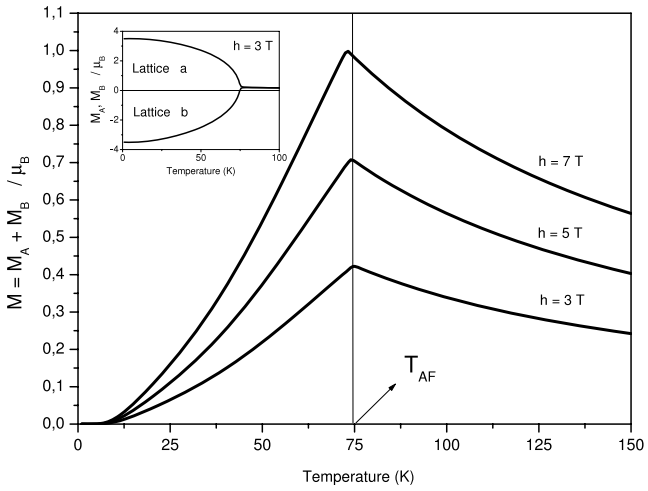


**Figure 1.** Magnetization versus temperature curves for applied magnetic fields $h = 3$, 5, and 7 T, calculated using the model parameters: $p = q = 1/2$, $g_a = g_b = 2$, $J_a = J_b = 7/2$, $\gamma_{aa} = \gamma_{bb} = 61.1\ \mathrm{T^2\ meV^{-1}}$, and $\gamma_{ab} = -122.2\ \mathrm{T^2\ meV^{-1}}$ (antiferromagnetic phase with $T_{\mathrm{AF}} = 75$ K). The inset shows the two sublattice magnetizations, $M_a$ and $M_b$ versus temperature for magnetic field $h = 3$ T.

## 3. Model application and discussions

### *3.1. MCE in antiferromagnetic systems*

In the simplest form of an antiferromagnetic system, the lattice of magnetic ions can be divided into two equivalent interpenetrating sublattices ($a$) and ($b$) such that ($a$) ions have only ($b$) ions as nearest neighbors, and vice versa with the magnetic moment saturated antiparallel at absolute zero temperature. In order to simulate an antiferromagnetic system using the model discussed above, the following model parameters were adopted: $g_a = g_b = 2$; $J_a = J_b = 7/2$ (which correspond, for example, to the Landé and total angular moment number for the gadolinium free ion); $\gamma_{aa} = \gamma_{bb} = 61.1\ \mathrm{T^2\ meV^{-1}}$, $\gamma_{ab} = -122.2\ \mathrm{T^2\ meV^{-1}}$ (these values leads to the Néel temperature $T_{\mathrm{AF}} = 75$ K, see relation (11)) and $p = q = 1/2$ (an equal number of up and down spins in the two sublattices ($a$) and ($b$), as it should be in antiferromagnetic system).

Figure 1 shows the temperature dependence of the net magnetization $M = M_a + M_b$ for different values of the external magnetic field, namely $h = 3$, 5, and 7 T. As the temperature increases, the thermal energy reduces the spontaneous magnetization in both sublattices ($a$) and ($b$), as shown in the inset of figure 1. Nevertheless, applying the external magnetic field on the magnetic moment direction of the ($a$)—magnetic moment ions leads to an increase of the net magnetization with temperature until $T_{\mathrm{AF}}$. Above $T_{\mathrm{AF}}$ the thermal energy effect overcomes the field alignment magnetic energy and $M$ decreases with temperature. It is worth noticing that $T_{\mathrm{AF}}$ decreases with intensity of the magnetic field.

Figure 2 shows the temperature dependence of $-\Delta S$ for magnetic field changes $\Delta h$: $0 \rightarrow 5$, 10, 15 T considering the same model parameters used in the construction of curves in figure 1. As expected, the negative values for $-\Delta S$ versus

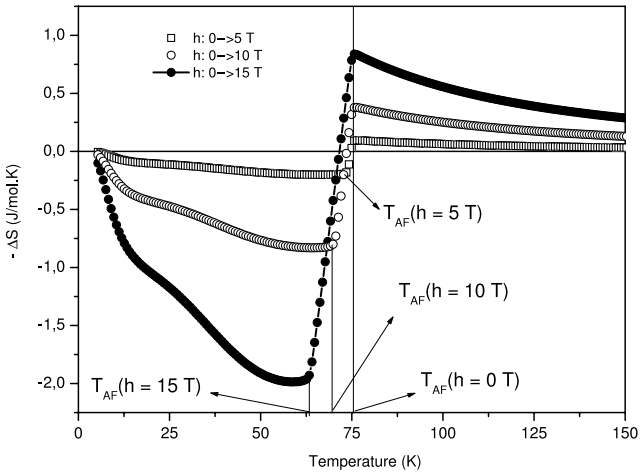


**Figure 2.** Magnetic entropy changes, $-\Delta S$, versus temperature (in an isothermic process) for applied magnetic field changes: $h = 0$–5, 0–10 and 0–15 T, calculated using the model parameters: $p = q = 1/2$, $g_a = g_b = 2$, $J_a = J_b = 7/2$, $\gamma_{aa} = \gamma_{bb} = 61.1$ T$^2$ meV$^{-1}$, and $\gamma_{ab} = -122.2$ T$^2$ meV$^{-1}$ (antiferromagnetic phase with $T_{\rm AF} = 75$ K).

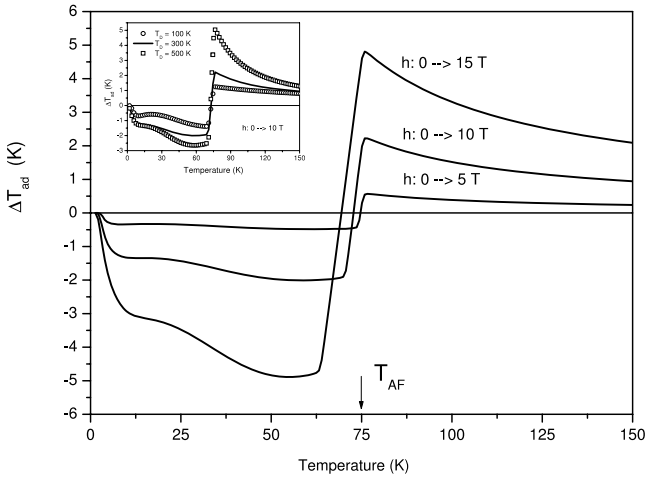


**Figure 3.** Adiabatic temperature changes, $\Delta T_{\rm ad}$, versus temperature for applied magnetic field changes: $\Delta h = 0$–5, 0–10 and 0–15 T, calculated using the model parameters: $p = q = 1/2$, $g_a = g_b = 2$, $J_a = J_b = 7/2$, $\gamma_{aa} = \gamma_{bb} = 61.1$ T$^2$ meV$^{-1}$, $\gamma_{ab} = -122.2$ T$^2$ meV$^{-1}$, and $T_{\rm D} = 300$ K (antiferromagnetic phase with $T_{\rm AF} = 75$ K). The inset shows the $\Delta T_{\rm ad}$ versus $T$, for $h = 10$ T considering different values for the Debye temperatures: $T_{\rm D} = 100$, 300, and 500 K.

$T$ curves appear below the Néel temperature, $T_{\rm AF} = 75$ K, since the derivative of $M$ versus $T$ presents a positive sign, see Maxwell relation (12). Above $T_{\rm AF} = 75$ K, in the paramagnetic phase region, the typical decreasing profiles of $-\Delta S$ versus $T$ curves are observed. A very interesting behavior in $-\Delta S$ versus $T$ curves is predicted to occur when the magnetic field intensity increases. Two regions can be identified which we call the nonlinear and linear in the $-\Delta S$ versus $T$ profile. In the non-linear region the modulus of $\Delta S$ increases in a nonlinear fashion up to the Néel temperature in the presence of applied magnetic field, $T_{\rm AF}(h)$. The linear region occurs in the temperature interval $T_{\rm AF}(h) < T < T_{\rm AF}$ $(h = 0)$. In this region $-\Delta S$ varies linearly with temperature and changes sign in this interval. For the magnetic field changes considered $\Delta h$: $0 \rightarrow 5$, 10, and 15 T, the temperature intervals of the linear regions are $\Delta T^{\rm Linear}$: 1.3, 5.4, and 11.7 K, respectively. It is worth noticing that linear temperature interval increases almost in the same proportion as the peak in the $-\Delta S$ versus $T$ curves.

Figure 3 shows the temperature dependence of $\Delta T_{\rm ad}$ for magnetic field changes $\Delta h$: $0 \rightarrow 5$, 10, and 15 T for the same model parameters considered above. These curves were calculated using relation (13) which requires the heat capacity function. For simplicity only magnetic and lattice entropy was considered, i.e. $C_h(T, h) = C_{\rm mag}(T, h) + C_{\rm latt}(T)$. The $C_{\rm mag}$ as discussed above, was obtained from the temperature derivative of the thermodynamic mean value of the Hamiltonian (1) and introduced in the relation (13) under the self-consistent condition, and the lattice entropy was considered in the Debye approximation with Debye temperature $T_{\rm D} = 300$ K. Above the Néel temperature, i.e. in the paramagnetic region, the $\Delta T_{\rm ad}$ versus $T$ curves present the usual behavior, where $\Delta T_{\rm ad}$ decreases smoothly to zero with temperature. Below the Néel temperature the inverse magnetocaloric effect occurs. The inverse MCEs were observed in several antiferromagnetic material measurements (see [16, 20, 23, 26–28]), but as far as we know, it was never simulated using a self-consistent microscopic model. Nevertheless, the inverse MCE is expected to occur from the general thermodynamic relation (13) in which a negative sign appears and all thermodynamic quantities are positive (note that the derivative of $M$ versus $T$ in the antiferromagnetic region is positive, see figure 1). The inset of figure 3 shows the influence of the Debye temperature on $\Delta T_{\rm ad}$ versus $T$ for magnetic field change $\Delta h$: $0 \rightarrow 10$ T. The solid curve in the inset was calculated using $T_{\rm D} = 300$ K and the circles and squares represent the $\Delta T_{\rm ad}$ versus $T$ curves using $T_{\rm D} = 100$ K and $T_{\rm D} = 500$ K, respectively. As the Debye temperature increases, the lattice contribution to the heat capacity decreases and consequently the $\Delta T_{\rm ad}$ increases as expected [30] from relation (13). As the Debye temperature increases from $T_{\rm D} = 100$ to 300 K a comparable increases in $\Delta T_{\rm ad}$ above and below the Néel temperature is observed. On the other hand, when the Debye temperature increases from $T_{\rm D} = 300$ to 500 K, a high change is observed above the Néel temperature compared with the small change below the Néel temperature.

### *3.2. MCE in ferromagnetic systems*

Figure 4 shows the temperature dependence of the $-\Delta S$ (scale on the left vertical axis) and $\Delta T_{\rm ad}$ (scale on the right vertical axis) for magnetic field change $\Delta h$: $0 \rightarrow 5$ T. These curves were obtained from the above model, only changing the exchange interaction $\gamma_{ab}$ from $\gamma_{ab} = -122.2$ to 61.1 T$^2$ meV$^{-1}$. Therefore, since now $\gamma_{aa} = \gamma_{bb} = \gamma_{ab}$ the ferromagnetic nature is imposed on the model Hamiltonian. Solving the magnetic state equations (8) and (9), we obtain the typical ferromagnetic curve (not shown in this work) for the net magnetization $M = M_a + M_b$ with saturation magnetization $M(T = 0) = 7\mu_{\rm B}$ and Curie temperature $T_{\rm FE} = 50$ K.

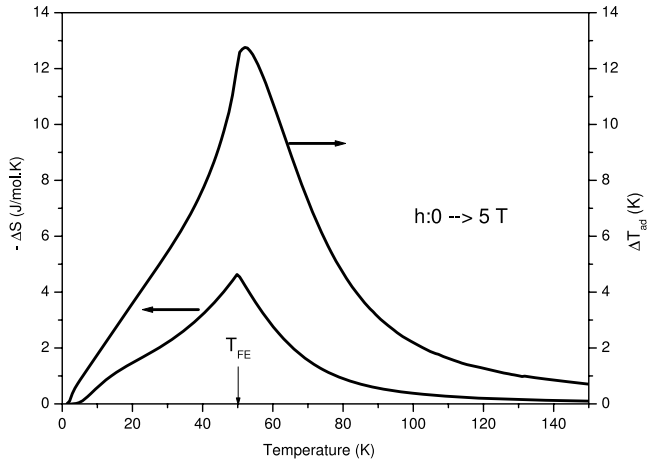


**Figure 4.** Magnetic entropy changes, $-\Delta S$, (left scale) (in an isothermic process) and adiabatic temperature changes, $\Delta T_{\rm ad}$, (right scale) versus temperature for applied magnetic field changes $\Delta h = 0$–10 T, calculated using the model parameters: $p = q = 1/2$, $g_a = g_b = 2$, $J_a = J_b = 7/2$, $\gamma_{aa} = \gamma_{bb} = \gamma_{ab} = 61.1$ T$^2$ meV$^{-1}$ (ferromagnetic phase with $T_{\rm FE} = 50$ K), and $T_{\rm D} = 300$ K.

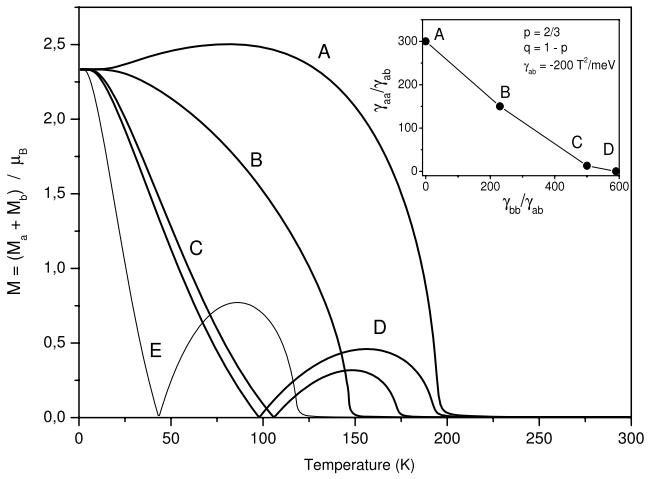


**Figure 5.** Magnetization versus temperature curves in ferrimagnetic phases, calculated using the model parameters: $\gamma_{aa} = 300$, $\gamma_{bb} = 0$, and $\gamma_{ab} = -200$ T$^2$ meV$^{-1}$ (curve A); $\gamma_{aa} = 150$, $\gamma_{bb} = 230$, and $\gamma_{ab} = -200$ T$^2$ meV$^{-1}$ (curve B); $\gamma_{aa} = 13$, $\gamma_{bb} = 500$, and $\gamma_{ab} = -200$ T$^2$ meV$^{-1}$ (curve C); $\gamma_{aa} = 0$, $\gamma_{bb} = 590$, and $\gamma_{ab} = -200$ T$^2$ meV$^{-1}$ (curve D); $\gamma_{aa} = 10$, $\gamma_{bb} = 400$, and $\gamma_{ab} = -80$ T$^2$ meV$^{-1}$ (curve E). All the other model parameters are common for all the curves $p = 2/3$, $q = 1/3$, $g_a = g_b = 2$, $J_a = J_b = 7/2$.

This Curie temperature is in accordance, as expected, with the value that comes from the analytical relation $T_{\rm FE} = C\gamma$ presented before. The maximum values of the MCE (in both curves $-\Delta S$ and $\Delta T_{\rm ad}$ in a ferromagnetic system) occur at the Curie temperature. Comparing the $-\Delta S$ curves in the antiferromagnetic and ferromagnetic regimes, we conclude that much more MCE is extracted at the ferro-paramagnetic phase transition than in the antiferro-paramagnetic phase transition. However, for antiferromagnetic materials, the MCE can occur in a broad temperature range which can be of practical interest. Physically it is expected since the ferromagnetic configuration presents less entropy than the antiferromagnetic one (considering ions with the same values of total angular moment) and in the paramagnetic phase the maximum magnetic entropy depends only on the total angular moment number $S^{\rm Max.}_{\rm mag} = R\ln(2J+1)$.

### *3.3. MCE in ferrimagnetic systems*

Even for the two sublattice system discussed above, there are several schemes that can lead to ferrimagnetic arrangements. We investigate here the ferrimagnetism arrangement in which all the magnetic ions have identical magnetic moment magnitudes, regardless of whether they are on the $a$-up sublattice or on the $b$-down sublattice, but with the fraction of $a$-ions with up spins, different from the fraction of $b$-ions with down spins, i.e. ($p \neq q$), which leads to the non-compensation magnetic moment in the magnetic system, therefore the system will possess a net moment $M = M_a + M_b \neq 0$. This case was treated in detail by Néel [31], and a particular case considering ($p = q$) basically reduces this ferrimagnetic arrangement to the antiferromagnetic one, presented above.

In order to study the MCE in the ferrimagnetic arrangement discussed above, we consider the following fixed model parameters: $g_a = g_b = 2$; $J_a = J_b = 7/2$; $p = 2/3$, and $\gamma_{ab} = -200$ T$^2$ meV$^{-1}$. Several different profiles for the temperature dependence of the net magnetization $M$ can be obtained by the variation of the intensity of the intra-sites exchange interactions $\gamma_{aa}$ and $\gamma_{bb}$. Figure 5 shows $M$ versus $T$ curves considering the following model parameters, represented by the coordinated pair ($\gamma_{aa}$, $\gamma_{bb}$): curve A (300, 0), curve B (150, 230), curve C (13, 500), curve D (0, 590). These curves were obtained numerically by the self-consistency procedure and the ordered–disordered phase transition temperatures were observed at $T_{\rm FI} = 194.26$ K, 146.5 K, 172.4 K, and 192 K, respectively. These critical phase transition temperatures, emerging from the numerical calculations, are in complete accordance with those calculated from the analytical relation (10), as expected. The inset of figure 5 shows the normalized coordinate points ($\gamma_{aa}/\gamma_{ab}$, $\gamma_{bb}/\gamma_{ab}$) which measure the intensity of the intra-sites exchange interaction in the $a$- and $b$-sites relative to the inter-site exchange interaction, for the four curves considered. The curve A presents, below $T = 90$ K, an increase of the net magnetization $M$ with temperature. This unusual shape occurs when the molecular field on $b$-site ions is less than on $a$-site ions, as a result $M_b$ decreases more rapidly with temperature than $M_a$ and, therefore, the net magnetization $M = M_a + M_b = |M_a| - |M_b|$ increases. The curve B has a usual profile where the magnetization decreases with increasing temperature (like the ferromagnetic profile). The curves C and D present the so-called ferrimagnetic compensation temperature ($T_{\rm comp}$) where the net magnetization vanishes since both sublattices present the same non-zero intensity magnetization $|M_a| = |M_b|$ with opposite directions. The curve E was obtained considering the following model parameters $\gamma_{ab} = -80$ T$^2$ meV$^{-1}$, $\gamma_{aa} = -10$ T$^2$ meV$^{-1}$ and $\gamma_{bb} = 400$ T$^2$ meV$^{-1}$. The curve E presents $T_{\rm comp} \sim 43$ K and $T_{\rm FI} = 117.6$ K and a high value of magnetization (of

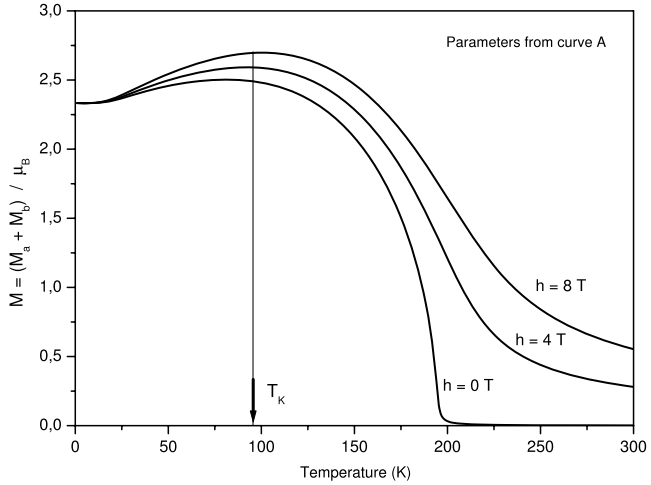


**Figure 6.** Magnetization versus temperature curves for applied magnetic fields $h = 0$, 4, and 8 T, calculated using the model parameters: $p = 2/3$, $q = 1/3$, $g_a = g_b = 2$, $J_a = J_b = 7/2$, $\gamma_{aa} = 300$, $\gamma_{bb} = 0$, and $\gamma_{ab} = -200$ T$^2$ meV$^{-1}$ (ferrimagnetic phase).

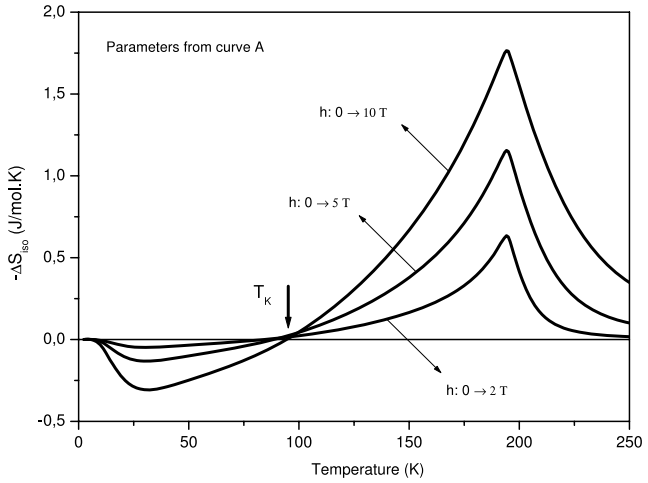


**Figure 7.** Magnetic entropy changes, $-\Delta S$ versus temperature (in an isothermic process) for applied magnetic field changes: $\Delta h = 0$ to 2, 0 to 5, and 0 to 10 T, calculated using the model parameters: $p = 2/3$, $q = 1/3$, $g_a = g_b = 2$, $J_a = J_b = 7/2$, $\gamma_{aa} = 300$, $\gamma_{bb} = 0$, and $\gamma_{ab} = -200$ T$^2$ meV$^{-1}$ (ferrimagnetic phase).

about 0.8 $\mu_B$) between $T_{comp}$ and $T_{FI}$. The parameters that were considered for the construction of curve E will be used below in the study of the MCE, where the compensation temperature exists.

Figure 6 shows the temperature dependence of the net magnetization, considering the model parameters of curve A for applied magnetic fields $h = 0$, 4, and 8 T. For temperatures below, approximately, $T_k = 95$ K (see the arrow in figure 6), the magnetization decreases with temperature decreasing, as expected, since the $b$-sublattice presents $\gamma_{bb} < \gamma_{aa}$. It is worth noticing that increasing the magnetic field leads to an increase of the temperature derivative of the magnetization curves below $T_k$.

Figure 7 shows the temperature dependence of $-\Delta S$ considering the same model parameters from curve A for magnetic field changes from 0 to 2 T, 0 to 5 T, and 0 to 10 T. The negative values for $-\Delta S$ occur below $T_k = 95$ K (see the arrow in figure 7). Above $T_k$, the $-\Delta S$ curves present positive values increasing with temperature up to $T_{FI} = 194.26$ K, and above this temperature smooth decreases in $-\Delta S$ curves are observed. The negative values of $-\Delta S$ below $T_k$ occur due to the positive temperature derivative of the magnetization below $T_k$ (see figure 6 and relation (12)). Above $T_k$ the temperature derivative of the magnetization is negative, leading to positive values for $-\Delta S$ versus temperature curves. The minimum values in the $-\Delta S$ curves in figure 7 depend on the magnetic field intensity ($-\Delta S_{min.} = -0.05$, $-0.13$ and $-0.3$ J mol$^{-1}$ K$^{-1}$ for magnetic field changes from 0 to 2 T, 0 to 5 T, and 0 to 10 T, respectively). The minimum values in $-\Delta S$ occur around $T = 30.3$ K at which the maximum temperature derivative of the magnetization, in the temperature interval between $T = 0$ K and $T_k$, occurs. We should mention that all the $-\Delta S$ versus temperature curves presented in this work, calculated using the integral calculation given by the relation (12), were confirmed by using the analytical relation (16) obtained for the two sublattice magnetic

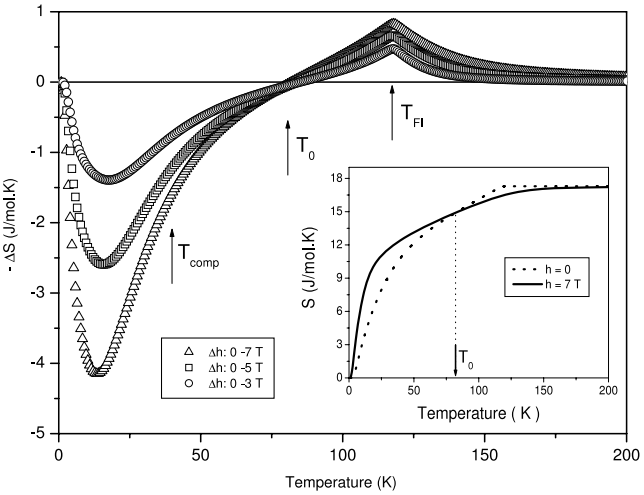


**Figure 8.** Magnetic entropy changes (in an isothermic process), $-\Delta S$, versus temperature for applied magnetic field changes: $\Delta h = 0$–3, 0–5, and 0–7 T, calculated using the model parameters: $p = 2/3$, $q = 1/3$, $g_a = g_b = 2$, $J_a = J_b = 7/2$, $\gamma_{aa} = 10$, $\gamma_{bb} = 400$, and $\gamma_{ab} = -80$ T$^2$ meV$^{-1}$. (ferrimagnetic phase). The inset shows the magnetic entropy versus temperature for magnetic field $h = 0$ (dotted curve) and for $h = 7$ T (solid curve).

entropies. Particular attention must be taken in the MCE calculation in order to be consistent with both formulations presented in relations (12) and (16): the magnetization that appears in relation (12) is not the modulus of the sublattice magnetization sum $|M_a + M_b|$ as usually considered in the plotting of ferrimagnetic systems, as in our figure 5. The proper magnetization value is $M = M_a + M_b$, which can be negative.

Figure 8 shows the temperature dependence of $-\Delta S$ curves, using the same model parameters considered for curve E in figure 7, for magnetic field changes from 0 to 3 T (circles), 0 to 5 T (squares), and 0 to 7 T (triangles). The high absolute values of the $-\Delta S$ curves are present at low

temperature $T \sim 13$ K and are associated with the high net magnetization changes at about ($\Delta M = 2.4\ \mu_B$) below the compensation temperature. It is worth noticing that the absolute $-\Delta S$ peak value, for magnetic field change from 0 to 5 T, is 2.6 J mol$^{-1}$ K$^{-1}$, which is smaller than the $-\Delta S$ peak obtained for the same magnetic field change in a ferromagnetic configuration 4.6 J mol$^{-1}$ K$^{-1}$ (see figure 4). The second and lower peaks are observed in the $-\Delta S$ curves at the ferri-paramagnetic phase transition $T_{FI} = 117.6$ K (see the arrow in figure 8).

The inset in figure 8 shows the temperature dependence of the magnetic entropy without magnetic field (solid curve) and with 7 T magnetic fields (dotted curve), obtained from relation (16). The $-\Delta S$ curves have a zero value between the $T_{comp}$ and $T_{FI}$ which occurs exactly at the temperature $T_0$ where the maximum magnetization values appear, see curve E in figure 5 and the relation (12). In our case, $T_0 = 82$ K (see the inset of figure 8) and this temperature separates the normal magnetocaloric effect from the inverse magnetocaloric effect. In other words, ferrimagnetic systems which present compensation temperature absorb heat below $T_0$ and release heat above $T_0$ under magnetic field application.

Figure 9 shows the temperature dependence of $\Delta T_{ad}$ for magnetic field changes from 0 to 3, 0 to 5, and 0 to 7 T using the same magnetic model parameters considered in the calculation of $-\Delta S$ versus $T$ in figure 8. The lattice entropy was taken in the Debye assumption with the Debye temperature $T_D = 300$ K (the same value adopted in the $\Delta T_{ad}$ calculation for the antiferromagnetic and ferromagnetic configurations, displayed in figures 3 and 4). The magnitude of the $\Delta T_{ad}$ peak at low temperature presents almost double the value of the $\Delta T_{ad}$ peaks at $T_{FI}$ for the corresponding magnetic field change. As expected, the inverse magnetocaloric effect is registered in the $\Delta T_{ad}$ versus $T$ curve for ferrimagnetic configuration below $T_0$ where the maximum magnetization occurs between $T_{comp}$ and $T_{FI}$ (at $T_0$ the temperature derivative of the magnetization is zero in both expression (12) and (13) which corresponds to the crossing between entropy curves with and without applied magnetic field shown in the inset of figure 8). In this way, a ferrimagnetic system which presents a compensation temperature is expected to cool down below $T_0$ and heat up above $T_0$ under magnetic field application.

The inset in figure 9 shows the influence of the Debye temperature on the two $\Delta T_{ad}$ versus $T$ peaks discussed above. The curve represented by squares is calculated with $T_D = 300$ K (the same as appears in figure 9), the dotted and solid curves were calculated using $T_D = 100$ K and $T_D = 500$ K, respectively. It should be noted that, for the considered magnetic model parameters, the increase of the Debye temperature is more relevant at inverse magnetocaloric temperature peaks than at the ferri-paramagnetic phase transition peaks.

## 4. Final comments

In this work a magnetic microscopic model, formed by two magnetic sublattices, which leads to different kinds of magnetic configurations, namely ferrimagnetic, antiferromagnetic, and ferromagnetic, was discussed by systematic changes of the model parameters. The influence of these magnetic configurations on the magnetocaloric effect was investigated using the sublattice self-consistent numerical procedure. This theoretical investigation allowed a better understanding of the inverse magnetocaloric effect observed in antiferromagnetic and ferrimagnetic materials. We must bear in mind that the origin of the inverse magnetocaloric effect is not only a consequence of the nature of the ferri-or antiferromagnetic configurations, for example, the paramagnetic intermetallic compound $PrNi_5$ presents the inverse MCE associated with crystalline electrical field level crossing [21, 22]. The simulations using the model discussed in this paper lead to several theoretical predictions for the magnetocaloric $-\Delta S$ and $\Delta T_{ad}$ quantities (curves profiles) as well as a systematic comparison between them.

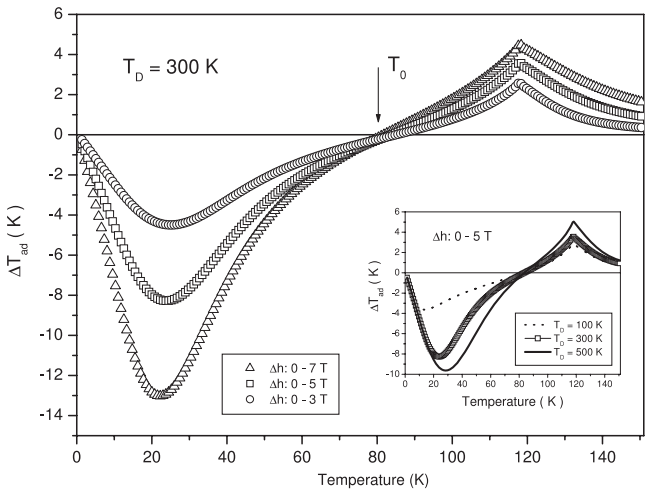


**Figure 9.** Adiabatic temperature changes, $\Delta T_{ad}$, versus temperature for applied magnetic field changes: $\Delta h = 0$ to 3, 0 to 5, and 0 to 7 T, calculated using the model parameters: $p = 2/3$, $q = 1/3$, $g_a = g_b = 2$, $J_a = J_b = 7/2$, $\gamma_{aa} = 10$, $\gamma_{bb} = 400$, $\gamma_{ab} = -80$ T$^2$ meV$^{-1}$ (ferrimagnetic phase), and $T_D = 300$ K. The inset shows the $\Delta T_{ad}$ versus $T$, for $\Delta h = 0$–5 T, considering different values for the Debye temperatures: $T_D = 100$, 300 K, and 500 K.

## Acknowledgments

We acknowledge financial support from CNPq—Conselho Nacional de Desenvolvimento Científico e Tecnológico—Brazil, FAPERJ—Fundação de Amparo à Pesquisa do Estado do Rio de Janeiro.

## References

[1] Pecharsky V K and Gschneidner K A Jr 1997 *Phys. Rev. Lett.* **78** 4494
[2] Brown G V 1976 *J. Appl. Phys.* **47** 3673
[3] Hashimoto T, Numazawa T, Shiino M and Okada T 1981 *Cryogenics* **21** 647
[4] Tegus O, Brück E, Buschow K H J and de Boer F R 2002 *Nature* **415** 150
[5] Wada H and Tanabe Y 2001 *Appl. Phys. Lett.* **79** 3302

[6] Wada H, Morikawa T, Taniguchi K, Shibata T, Yamada Y and Akishige Y 2003 *Physica* B **328** 114
[7] Hu F, Shen B, Sun J, Cheng Z, Rao G and Zhang X 2001 *Appl. Phys. Lett.* **78** 3675
[8] Fujita A, Fujieda S, Hasegawa Y and Fukamichi K 2003 *Phys. Rev.* B **67** 104416
[9] Bean C P and Rodbell D S 1961 *Phys. Rev.* **126** 104
[10] von Ranke P J, de Oliveira N A and Gama S 2004 *J. Magn. Magn. Mater.* **277** 78
[11] von Ranke P J, de Oliveira N A and Gama S 2004 *Phys. Rev.* B **70** 094410
[12] von Ranke P J, de Oliveira N A and Gama S 2004 *Phys. Lett.* A **320** 302
[13] Brück E 2005 *J. Phys. D: Appl. Phys.* **38** R381–91
[14] Gschneidner K A, Pecharsky V K and Tsokol A O 2005 *Rep. Prog. Phys.* **68** 1479
[15] Phan M-H and Yu S-C 2007 *J. Magn. Magn. Mater.* **308** 325
[16] Schelleng J H and Friedberg S A 1963 *J. Appl. Phys.* **34** 1087
[17] Schelleng J H and Friedberg S A 1969 *Phys. Rev.* **185** 728
[18] Kurti N 1951 *J. Phys. Radium* **12** 281
[19] Garrett C G B 1951 *Proc. R. Soc.* A **206** 242
[20] Clark A E and Callen E 1969 *Phys. Rev. Lett.* **23** 307
[21] von Ranke P J, Pecharsky V K, Gschneidner K A and Korte B J 1998 *Phys. Rev.* B **58** 14436
[22] von Ranke P J, Mota M A, Grangeia D F, Carvalho A M G, Gandra F C G, Coelho A A, Caldas A, de Oliveira N A and Gama S 2004 *Phys. Rev.* B **70** 134428
[23] Krenke T, Duman E, Acet M, Wassermann E F, Moya X, Mañosa L and Planes A 2005 *Nat. Mater.* **4** 450
[24] Krenke T, Acet M, Wassermann E F, Moya X, Mañosa L and Planes A 2005 *Phys. Rev.* B **72** 014412
[25] Pecharsky V K and Gschneidner K A Jr 2001 *Adv. Mater.* **13** 683
[26] Moya X, Mañosa L, Planes A, Aksoy S, Acet M, Wassermann E F and Krenke T 2007 *Phys. Rev.* B **75** 184412
[27] Sandeman K G, Daou R, Özcan S, Durrell J H, Mathur N D and Fray D J 2006 *Phys. Rev.* B **74** 184412
[28] Zhang Y Q and Zhang Z D 2004 *J. Alloys Compounds* **365** 35
[29] Samuel Smart J 1966 *Effective Field Theories of Magnetism* (Philadelphia, PA: Saunders) p 115
[30] Wolf W P 1961 *Rep. Prog. Phys.* **24** 212
[31] Néel L 1948 *Ann. Phys. Fr.* **3** 137